Single-Shot Flow Synthesis of D-Proteins for Mirror-Image Phage Display

Alex J. Callahan[1], Satish Gandhesiri[1], Tara L. Travaline[2], Lia Lozano Salazar[1], Stephanie Hanna[1], Yen-Chun Lee[1,a], Kunhua Li[2], Olena S. Tokareva[2], Jean-Marie Swiecicki[2], Andrei Loas[1], Gregory L. Verdine[2], John H. McGee[2*], Bradley L. Pentelute[1,3,4,5*]

[1]Department of Chemistry, Massachusetts Institute of Technology, 77 Massachusetts Avenue, Cambridge, MA 02139, USA

[2]FOG Pharmaceuticals Inc., 30 Acorn Park Drive, Cambridge, MA 02140, USA

[3]The Koch Institute for Integrative Cancer Research, Massachusetts Institute of Technology, 500 Main Street, Cambridge, MA 02142, USA

[4]Center for Environmental Health Sciences, Massachusetts Institute of Technology, 77 Massachusetts Avenue, Cambridge, MA 02139, USA

[5]Broad Institute of MIT and Harvard, 415 Main Street, Cambridge, MA 02142, USA

[a]*Current address*: Department of Chemistry, National Cheng Kung University, No.1, University Road, Tainan City 701, Taiwan

*Email: jmcgee@fogpharma.com, blp@mit.edu

Abstract

Mirror-image biological systems have the potential for broad-reaching impact in health and diagnostics, but their study has been greatly limited by the lack of routine access to synthetic D-proteins. We demonstrate that automated fast flow peptide synthesis (AFPS) can reliably produce novel mirror-image protein targets without prior sequence engineering. We synthesized 12 D-proteins, along with their L-counterparts. All 24 synthetic proteins were folded into active structures in vitro, and characterized using biochemical and biophysical techniques. From these chiral protein pairs, we chose MDM2 and CHIP to carry forward into mirror-image phage display screens, and identified macrocyclic D-peptides that bind the recombinant targets. We report 6 mirror-image peptide ligands with unique binding modes: three to MDM2, and three to CHIP, each confirmed with X-ray co-crystal structures. Reliable production of mirror-image proteins with AFPS stands to enable not only the discovery of D-peptide drug leads, but to the study of mirror-image biological systems more broadly.

Introduction

The biomolecules active in the central dogma: DNA, RNA, and proteins, are universally homochiral. Their unnatural enantiomers (L-DNA, L-RNA, and D-proteins) are the mirror-images of their natural counterparts, and still carry out their biochemical function, but with inverted enantiomeric selectivity[1,2]. Currently, these mirror-image biomolecules can only be accessed by total chemical synthesis; the molecular cloning techniques ubiquitous in modern biology necessitate a large repertoire of components that have not yet been produced in their mirror-image forms. Recent work[3,4] has underlined the critical need for reliable access to mirror-image proteins to enable the development of potential therapeutics and to further explore biotechnological applications of mirror-image systems. Accordingly, a major driver of new methods in protein chemical synthesis[5] has been to enable the routine access to D-proteins of useful length. To this end, we envisioned that a newly reported protein synthesis technique, automated flow peptide synthesis (AFPS)[6] could significantly increase the rate of D-protein production.

One of the foremost applications of D-proteins is in the discovery of biologically stable D-peptide ligands to the native L-protein [7]. Such ligands are starting points for development of molecular probes and drugs, given their extremely long half-lives within living systems[8], so their identification is a major area of research in academia and industry. One such technique to identify D-peptide ligands from synthetic D-proteins is mirror-image phage display (MIDP). A library of L-peptides displayed on phage surfaces are selected against a bait D-protein, and the resulting enriched peptide ligands when produced in their D form bind to the native L protein. First reported almost 30 years ago MIDP has been applied to a number of important protein targets, but has not yet been implemented broadly. As highlighted by the 2018 Nobel Prize awarded in part for the development of phage display, these display techniques have become ubiquitous, but examples of screening on D-proteins remain rare – to the best of our knowledge, MIDP has only been applied to nine protein targets[7,9–19] .

A significant limitation to the widespread adoption of mirror-image display platforms relates to the challenges associated with accessing useful amounts of the required synthetic D-proteins. Modern chemical synthesis techniques have enabled access to synthetic proteins, but are not always practical or sufficiently dependable[20,21]. Accessing sufficient amounts of folded synthetic protein to carry out phage display screening can require significant effort and expertise to define and optimize a suitable synthetic route. This is further complicated by the fact that the requisite protected D-amino acids are ~10-times more expensive than their L-counterparts[4]. Such considerations have driven the development of new methods to enhance access to synthetic proteins. We recently reported a protocol, we termed automated fast-flow peptide synthesis (AFPS, Fig. 1)[22], that utilizes highly optimized flow

chemistry to produce long peptides (> 50 AAs) with unmatched purity. With this protocol, we recently demonstrated the one-shot synthesis of proteins that had previously had taken days[6]. We anticipated that this technology could overcome sequence-dependent complications that are ubiquitous in the production of novel protein targets that would be of therapeutic interest.

Here, we applied AFPS to a panel of 12 diverse proteins, eight of which had not been previously synthesized by chemical methods in either chiral form, and used two target pairs to generate high-affinity peptide ligands. We could successfully isolate milligram amounts of 12 proteins in both L- and D-forms (24 total proteins) (Fig. 2). Taken together, these syntheses represent a major fraction of the total number of D-proteins reported in the past five years (12 out of 36 reported targets[2–4,11,12,16–18,23–31,31–37]). We aimed to apply a recently reported screening platform based on phage display to generate high-affinity conformationally constrained ("stapled") α-helical peptides, termed Helicons, in a single MIDP screening pass[38]. We used this platform to discover Helicons that bind to two of the D-proteins we synthesized here, MDM2 and CHIP. The resulting hits included a total of six distinct families of mirror-image Helicons, three to MDM2, and three to CHIP. Analysis of D-peptide-target X-ray co-crystal structures revealed in some cases similar side-chain interactions to known binders that utilize different structural scaffolds, including unstructured loops, and α-helices with opposite handedness. The rapid generation of high-affinity mirror-image binding modes made possible with AFPS coupled to modern Helicon phage display affinity selection represents a major advance in improving the throughput and general accessibility of MIPD, and is poised to revitalize campaigns to generate mirror-image binders to existing and emerging protein targets.

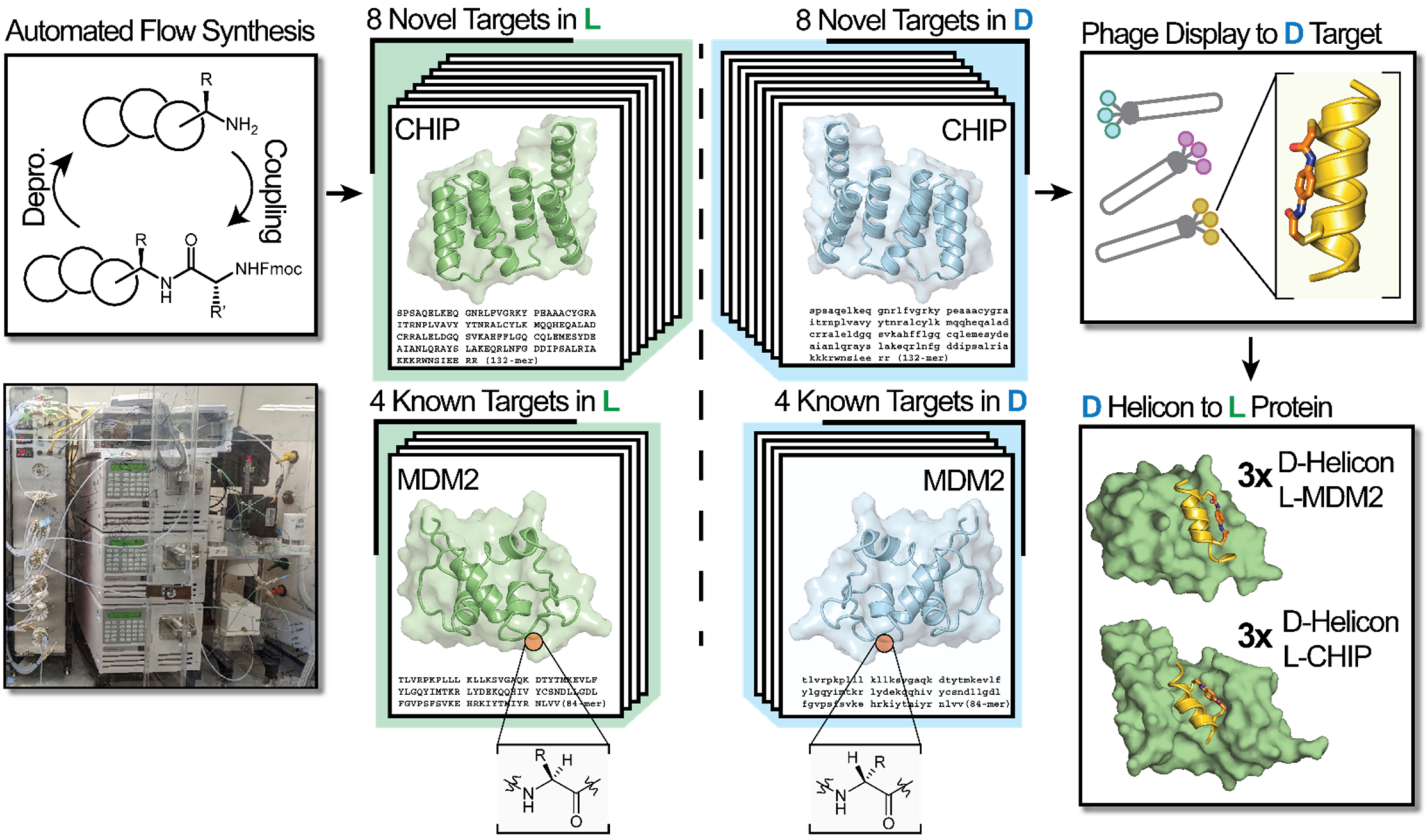

Figure 1. Rapid generation of D-peptide binders leverages automated flow protein synthesis coupled with mirror-image phage display. Automated flow protein synthesis can rapidly manufacture proteins with L- or D-amino acids. Subsequent folding and biochemical purification of each polypeptide chain affords synthetic protein pairs which are mirror-images of each other. Phage display screening of the D-protein enantiomer with stapled alpha-helical peptides, termed Helicons, can reveal sequences with low-micromolar binding affinity. Mirroring of the hit Helicons from L- to D-chirality affords binders to the native L-protein with the same affinity.

Results

Synthesis of enantiomeric protein pairs with AFPS

We first defined a panel of 12 structurally diverse single-domain proteins for generation of synthetic L- and D-versions using AFPS (Fig. 2). Two of these proteins, MDM2[10] and Barnase[39], were previously prepared in their all-D forms (see SI Sections 5.1 and 5.3), so can be used to assess the reliability and fidelity of the AFPS approach. We also chose two proteins that had previously only been synthesized in their native L-forms: Myc-Max, and Max-Max[40] (see SI Sections 5.11 – 5.17). We chose an additional eight single-domain proteins ranging in length from 70-132 amino acids with no reported chemical synthesis: ERG (PNT domain), (see SI Section 8.2) IRAK2 (death domain) (see SI Section 5.4), CHIP (tetranucleotide repeat domain) (see SI Section 5.5), NEMO (coiled coil domain) (see SI Section 5.6), FKBP12 (see SI Section 5.7), BCL11a (Zn finger domains) (see SI Section 5.8), YAP1 (ww1-ww2 domains) (see SI Section 5.9) and NEMO_iZIP (coiled coil domain with iZip adapters[41]) (see SI Section 5.10). In all cases, we appended a biotin unit at the N-terminus of the protein through a PEG_{12} linker to facilitate phage display screening.

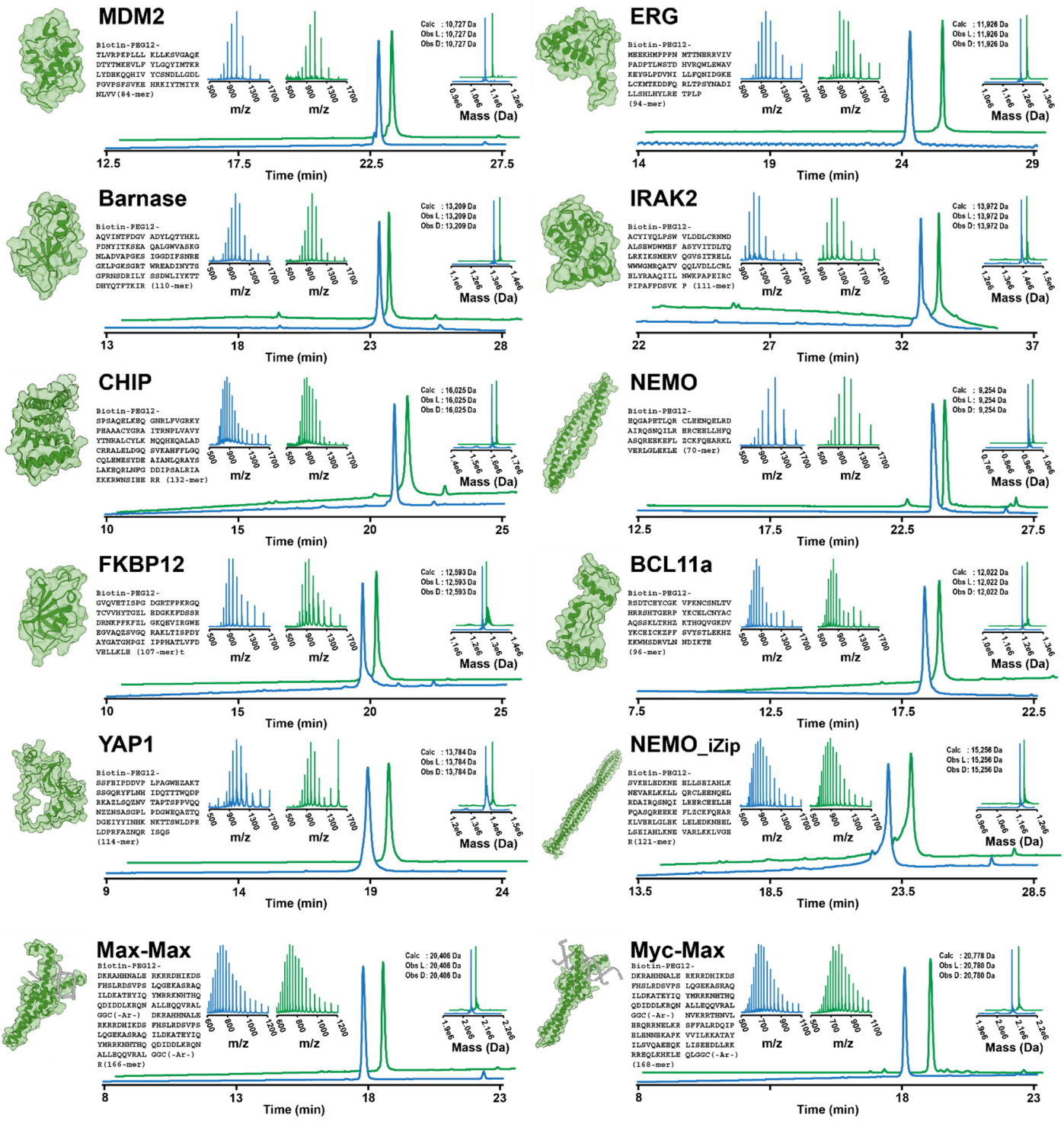

Figure 2. Automated flow synthesis delivers diverse single-domain protein chains in both enantiomeric forms. Analytical characterization of reverse phase-purified L- and D-chains from AFPS. Green traces show characterization of L-proteins, and blue traces show characterization of D-proteins. For each protein target, the following data are shown: (1) analytical HPLC trace of purified material recorded at 214 nm (bottom overlayed chromatograms); (2) total ion current (TIC) post-injection on a Q-TOF LC-MS instrument (separate insets on the left); and (3) the deconvolution of the TIC traces of (2) shown as overlayed insets on the right. Observed masses from the deconvolution are shown along with the predicted values. Previously reported structures are depicted for each of the targets, sourced from prior X-ray crystal structures, NMR structures, or Alphafold predictions[42,43] (MDM2: 3FDO, ERG: 1SXE, Barnase: 1A2P, IRAK2: 3MOP CHIP: 4KBQ, NEMO: 3BRV, FKBP12: 2PPN, BCL11a: 6KIK,

YAP1: Alphafold prediction of Uniprot ID P46937 region 63-276, NEMO_iZIP: 6MI3, Myc-Max: 1HLO, Max-Max: 1NKP).

We used AFPS to prepare each polypeptide chain in a stepwise fashion, with total synthesis times ranging from 4-7 hours, using three separate AFPS instruments. After we released the proteins from the H-Rink Amide solid support, we isolated them by precipitation with cold diethyl ether (see SI Sections 3 and 2.3). We used analytical reverse phase HPLC (RP-HPLC) and liquid chromatography–mass spectrometry (LC-MS) to analyze crude peptide mixtures and preparative mass-directed RP-HPLC to purify them. We typically obtained ~5 μmol of crude polypeptide powder from individual synthesis runs, and purifying ~3 μmol of this material afforded ~0.3 μmol of pure peptide. Gradient shape for the preparative purification was determined by a preliminary run at low protein loading on the same column used for purification (see SI Section 2.6). Typical yields are on the order of 1-10 mg (0.07–0.7 μmol, 0.3%–3% isolated yield based on resin loading). In all instances, a single synthesis experiment afforded sufficient material after folding for phage selections and biochemical validation.

Folding of diverse D-proteins with preparative size exclusion chromatography

Using a generalized folding protocol, each synthetic protein was folded to a homogeneous product as analyzed by size-exclusion chromatography (SEC). We set out to identify appropriate folding conditions for our 12 enantiomeric protein pairs and began by adopting the protocols that had been used to successfully isolate folded protein in aqueous solution for the few targets for which literature reports exist. Specifically, our group has previously isolated L/D Barnase[6] and L/D MDM2[44] via stepwise dilution from a high concentration of guanidine hydrochloride. Subsequent purification using semi-preparative SEC achieves yields ranging from 4.5 to 10.6 nmol for all four targets. Here, using this technique, we were unable to identify any dilution conditions under which we could isolate folded BCL11a or IRAK2. Instead, we observed significant precipitation for both target pairs, with any remaining solubilized material eluting in the exclusion volume of the column, indicating an apparent molecular weight at least 10-fold over the expected value, consistent with the formation of soluble aggregates.

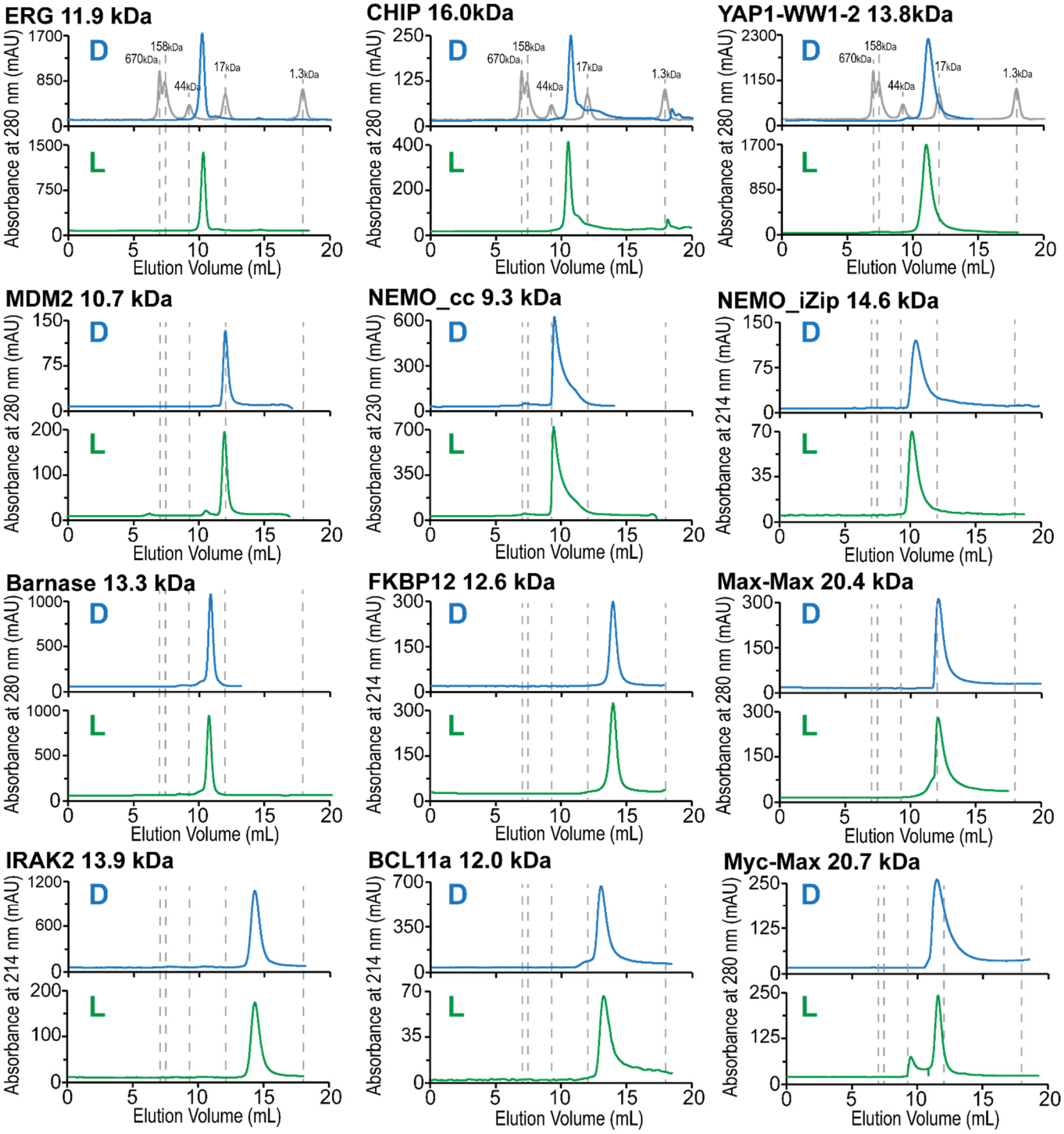

Figure 3. After folding, synthetic proteins obtained by AFPS are homogeneous by size exclusion chromatography. Analytical size exclusion chromatography traces are shown for each L- and D-protein described in Fig. 2. Samples were seperated on a Superdex 75 Increase 10/300 GL SEC column affixed to a Agilent BioInert HPLC system. For proteins with no trpytophan or low extinction coefficients, spectra were recorded at wavelengths that provided sufficient signal-to-noise – either 214 nm or 230 nm. Molecular weight standards – bovine thyroglobulin (670 kDa), bovine γ-globulin (158 kDa), chicken ovalbumin (44 kDa), horse myoglobin (17 kDa), vitamin B12 (1.3 kDa) – are overlayed in the traces in the top row, and vertical dotted lines denoting their respective elution times are overimposed on each subsequent chromatogram.

To address these complications, we adapted a refolding technique utilizing SEC to isolate the remaining protein targets. Purified proteins were dissolved in a denaturing buffer, typically a 10 mg / mL solution containing 6 M guanidine hydrochloride buffered to pH 7.5 with 50 mM 4-(2-hydroxyethyl)-1-piperazineethanesulfonic acid) (HEPES) and including 50 mM dithiothreitol (DTT). The mixture was then submitted to semi-preparative SEC coupled to an HPLC instrument. The denaturant is removed as the protein progresses through the SEC column, and the resulting folded protein can be separated from off-target aggregates based on their different retention times. The running buffer of the SEC could be tuned to the requirements of each particular protein, but unless otherwise specified was 50 mM HEPES, 150 mM NaCl, 0.5 mM DTT, 5% glycerol (v/v), at pH 7.5. DTT was omitted in cases where the protein contained no free sulfhydryl groups (NEMO, NEMO_iZIP, Myc-Max, and Max-Max). For BCL11a, which contains three Zn-finger motifs, both the denaturing buffer and the running buffer were adjusted to contain $ZnCl_2$ with additional alterations to prevent precipitation of Zn salts. In each case, the folding protocol afforded material as major elution peaks with retention times consistent with the calculated molecular weights (Fig. 3, SI Sections 7.1 to 7.12). This set includes BCL11a, and IRAK2 for which we were unable to isolate folded material by any other technique. Some proteins elute as peaks with apparent molecular weight larger than would be otherwise expected, including CHIP, NEMO, NEMO_iZIP, and BCL11a. In the case of NEMO, and NEMO_iZIP, this behavior has been established and has been attributed to their extended structures[41,45].

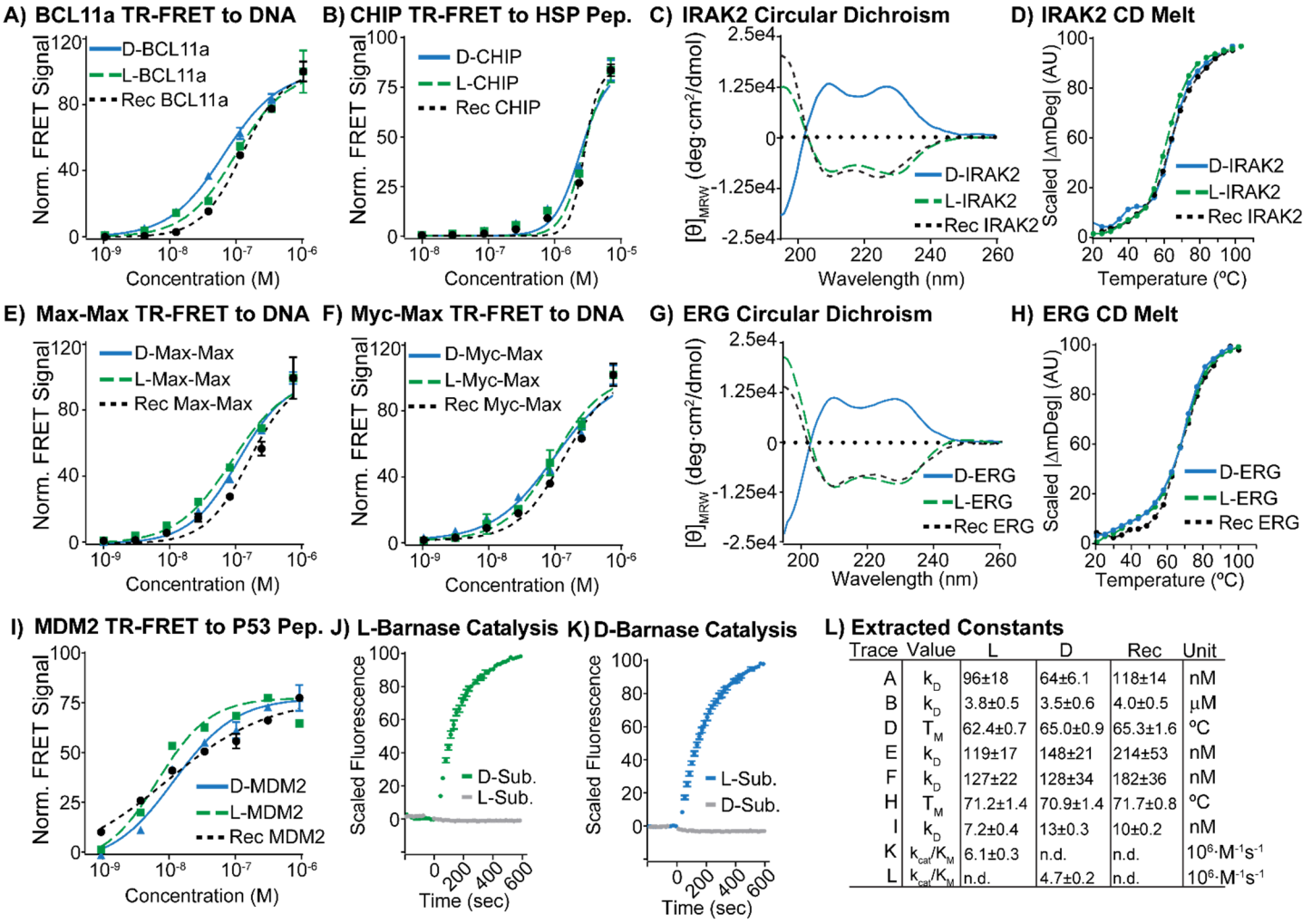

L) Extracted Constants

Trace	Value	L	D	Rec	Unit
A	k_D	96±18	64±6.1	118±14	nM
B	k_D	3.8±0.5	3.5±0.6	4.0±0.5	μM
D	T_M	62.4±0.7	65.0±0.9	65.3±1.6	ºC
E	k_D	119±17	148±21	214±53	nM
F	k_D	127±22	128±34	182±36	nM
H	T_M	71.2±1.4	70.9±1.4	71.7±0.8	ºC
I	k_D	7.2±0.4	13±0.3	10±0.2	nM
K	k_{cat}/K_M	6.1±0.3	n.d.	n.d.	$10^6 \cdot M^{-1}s^{-1}$
L	k_{cat}/K_M	n.d.	4.7±0.2	n.d.	$10^6 \cdot M^{-1}s^{-1}$

Figure 4. Synthetic D-proteins display similar biological activity to their synthetic L- and recombinant counterparts. Kinetic binding data for five synthetic protein targets to peptide ligands of the appropriate chirality are shown. Each of the shown D- and L-proteins display similar activity as their recombinant protein counterparts, and are consistent with literature reports of the same interactions. In all cases, experimental details are outlined in the Supporting Information. **A)** Synthetic D, L and recombinant BCL11a bind a model DNA oligonucleotide of the γ-globulin promoter[46] with similar affinity. The FAM-labeled oligonucleotide was incubated with varying concentrations of biotinylated BCCL11a and terbium-labeled streptavidin. The chirality of DNA substrate was adjusted to the chirality of the target (L-DNA to D-BCL11a, D-DNA to L-BCL11a). Binding was measured as an increase in FRET efficiency between the FAM and terbium streptavidin. **B)** Synthetic D, L and recombinant CHIP bind a peptide model of the heat shock protein 70 (Hsp70) C-terminus with similar affinity. The chirality of the peptide substrate was adjusted to the chirality of the target (D-peptide to D-CHIP, L-peptide to L-CHIP). The FAM-labeled HSP70 peptide was incubated with varying concentrations of biotinylated CHIP and terbium-labeled streptavidin, and binding was measured as described in **A**. **C)** Synthetic D, L and recombinant IRAK2 display similar proportions of secondary structure by near circular dichroism (CD). CD spectra were recorded from 195 to 260 nm over a 0.1 cm pathlength at a protein concentration of 0.1 mg/mL. **D)** Synthetic L, D and recombinant IRAK2 have similar melting temperatures (T_m) as determined by variable temperature CD. The absolute intensity of the CD spectrum at 222 nm of each protein was monitored from 20 °C to 100 °C in 5 °C steps. **E)** Synthetic D, L and recombinant Max-Max bind a model DNA oligonucleotide of E-box DNA[40] with similar affinity. The FAM labeled DNA was incubated with varying concentrations of biotinylated Max-Max, and terbium-labeled streptavidin. Binding was measured as described in **A**. The chirality of DNA substrate was adjusted to the chirality

of the target (L-DNA to D-Max-Max, D-DNA to L-Max-Max). **F)** Synthetic D, L and recombinant Myc-Max bind a model DNA oligonucleotide of E-box DNA[40] with similar affinity. The FAM labeled DNA was incubated with varying concentrations of biotinylated Myc-Max and terbium-labeled streptavidin. Binding was measured as described in **A**. The chirality of DNA substrate was adjusted to the chirality of the target (L-DNA to D-Myc-Max, D-DNA to L-Myc-Max). **G)** Synthetic D, L and recombinant ERG display similar proportions of secondary structural features by near circular dichroism (CD). CD spectra were recorded as described in **C**. **H)** Synthetic L, D and recombinant ERG have similar melting temperatures determined as described in **D**. **I)** Synthetic D, L and recombinant MDM2 bind a peptide model of the p53 protein with similar affinity. The FAM labeled p53 peptide was incubated with varying concentrations of biotinylated MDM2 and terbium-labeled streptavidin. Binding was measured as described in **A**. The chirality of peptide substrate was adjusted to the chirality of the target (D-peptide to D-MDM2, L-peptide to L-MDM2). **J)** and **K)** Synthetic L- and D-barnase, respectively, selectively catalyze the hydrolysis of a stereochemically matched RNA substrate. An RNA substrate labeled with FAM and TAMRA separated by a barnase cleavage site was prepared in both the L- and D-forms. Each substrate was incubated with L-barnase (**J**) and D-barnase (**K**), and catalytic activity was measured as an increase in fluorescence intensity after barnase addition. No cleavage for the mismatched substrate pairs (L-RNA to L-barnase and D-RNA to D-barnase) was observed. **L)** Table summarizing the experimentally determined binding constants, melting temperatures, and kinetic constants for the reported synthetic proteins (n.d. = not determined).

Synthetic D- and L-proteins display correct biochemical activity

For each enantiomeric pair generated using AFPS, we used biochemical assays to confirm that the activities of the synthetic proteins are similar to their recombinant versions. For proteins with known high-affinity binding partners, we measured the affinities of the synthetic proteins to fluorophore-tagged probes of the appropriate chirality using time-resolved fluorescence resonance energy transfer (TR-FRET). Binder substrates were modified with 5(6)-carboxyfluorescein (FAM), and the biotinylated target proteins were complexed with terbium-labeled streptavidin. Binding was measured as an increase in fluorescence quenching between the two fluorophores. For BCL11a binding to DNA (Fig. 4A and SI Section 8.1), CHIP binding to HSP peptide (Fig. 4B and SI Section 8.2), MDM2 binding to p53 peptide (Fig. 4I and SI Section 8.3), Max-Max binding to E-Box DNA (Fig. 4E and SI Section 8.4.1), and Myc-Max binding to E-Box DNA (Fig. 4F and SI Section 8.4.2), each synthetic chiral protein displayed apparent dissociation constants (K_D) for the L- and D-proteins to be consistent with those of the recombinant proteins (Fig. 4M). We next used surface plasmon resonance (SPR) binding assays with substrates of the matching chirality to asses binding of NEMO to iKKb peptide (see SI Section 8.7), NEMO_iZip binding to iKKb peptide (see SI Section 8.10), YAP1 binding to dendrin (see SI Section 8.9), and L-FKBP12 binding to Rapamycin followed by mTOR (see SI Section 8.8). Again, in all instances, the synthetic proteins displayed binding affinities similar to the recombinantly derived proteins, suggesting that the synthetic proteins derived from AFPS are folding into bioactive tertiary structures.

Synthetic L/D barnase from AFPS displays ribonucleolytic activity that is selective for the chirality of its nucleotide substrate. Barnase catalytically cleaves a fluorescently quenched reporter RNA substrate[47] composed of a tetranucleotide flanked with FAM and 6-carboxytetramethylrhodamine (6-TAMRA) labels on either end (FAM-DdA-DrU-DdA-DdA-TAMRA), where each nucleotide is specified as the L- or D-enantiomer and the ribose (r) or deoxyribose (d) sugar. We tracked the barnase-mediated cleavage of substrate by assessing the FRET between the FAM and TAMRA fluorophores, which is abolished upon cleavage. When the chirality of the substrate and protein were matched, as for L-barnase to the D-substrate FAM-DdA-DrU-DdA-DdA–TAMRA, and D-barnase to the L-substrate FAM-LdA-LrU-LdA-LdA–TAMRA, we observed rapid hydrolysis with extracted kinetic constants that are similar to previously reported values (Fig. 4J,K)[39]. In the mismatched cases, L-barnase to L-substrate and D-barnase to D-substrate, we observed no catalysis on the timescale of our observation (Fig. 4J,K) (see SI Section 8.5). These results reconfirm the structural and biological integrity of the folded synthetic proteins, indicating that their enantiomeric purities are retained throughout the synthesis and purification processes.

For protein targets with no known binding partners and no available assays to assess enzymatic activity exists (ERG and IRAK2), we recorded circular dichroism (CD) spectra and compared them to recombinantly derived material. Both targets are reported to be mostly alpha-helical[48,49], and we could confirm this for the recombinant proteins. The CD spectra for the synthetically derived L-proteins closely matched those of the recombinant versions, indicating that the synthetic material is forming secondary structures in similar proportions (Fig. 4C and G) (see SI Section 8.6.1). Both D-ERG and D-IRAK2 display a CD signal with similar absolute intensities as the corresponding synthetic L- and recombinant proteins, but with inverted sign, consistent with the formation of mirror-image secondary structures. Furthermore, we found that both synthetic protein pairs form folded structures with melting temperatures (*Tm*) close to those of the recombinantly derived protein, as shown by tracking the intensity of the α-helical signature as a function of temperature (Fig. 4D and H) (see SI Section 8.6.2). Together, these data suggest that the synthetically derived L/D ERG and L/D IRAK2 form tertiary structures that closely resemble the native proteins.

Generation of D-peptide ligands using mirror-image phage display

Having validated the structure and function of our synthetic D-proteins, we next set out to identify unique D-peptide binders to the corresponding native proteins using our next-generation MIPD platform[38]. We were able to screen two immobilized synthetic protein targets, MDM2 and CHIP, simultaneously in a single round of screening using an unbiased phage library of 10^8 members that display macrocyclic α-helical peptides (Helicons). We sequenced phage particles that remained bound

to the targets after washing using next-generation sequencing. Comparisons of sequencing reads to a spiked-in internal reference allowed for a semi-quantitative read-out of binding affinity as a function of protein bait concentration (see SI Section 2.7). The resulting hit sequences that displayed proper dose-response were clustered into binder families using hierarchical statistical clustering.

Previous work has identified D-peptide ligands to MDM2[10], and we set out to investigate if we could recapitulate these sequences and further discover novel binding motifs. From a single-round screen, we identified three binding clusters (MDM2.C1-MDM2.C3) selective for D-MDM2 (Fig. 5A and SI Section 9.1). Consistent with previously described α-helical peptide binders to MDM2[50,51], all three clusters contain anchoring N-terminal tryptophan residues(dW2 in MDM2.C1, dW1 in MDM2.C2, and dW1 in MDM2.C3), and show conserved hydrophobic residues on the same α-helical face as the tryptophan(*i*,*i*+4/5 and *i*,*i*+8/9 relative to dW on each cluster). To validate the specificity of each binding cluster, we synthesized representative binding peptides in the D-form (D-H101 from MDM2.C1, D-H102 from MDM2.C2, and D-H103 from MDM2.C3) and measured binding with SPR against recombinant MDM2. We observed binding constants of 5.5 μM, 2.4 μM, and 0.88 μM, respectively, as determined by SPR assays using recombinant MDM2 (Fig. 5B-D and SI Section 8.11).

To further investigate the binding modes of each binding cluster, we solved the X-ray co-crystal structures of D-H101 (Fig. 5B, 1.64 Å), D-H102 (Fig. 5C, 1.30 Å), and D-H103 (Fig. 5D, 1.90 Å) with recombinant MDM2 (see SI Sections 10.1 and 10.3). All three peptides form left-handed α-helices that engage the same hydrophobic groove on MDM2, but make use of different side chain interactions. In particular, D-H101 and D-H102 use similar amino acids to interact with MDM2 at its N-terminus (dW5/dW4, dY6/dH6, and dF9/dY9), but diverge towards the C-terminus where the side-chain conformations are altered (dQ12/dF12, dV13/dV13, and dE16/dF16) (Fig. 5B-C). Beyond the conserved N-terminal aromatic residues, D-H103 makes use of substantially different side-chain interactions than either D-H101 or D-H102. (Fig. 5D vs Fig. 5B-C).

Consistent with their sequence similarities, D-H101 utilizes similar side-chain interactions to two previously reported α-helical peptide binders to MDM2. Overlay of the known D-peptide MDM2 binder dPMI[1-5, 9-12][50] onto the D-H101 MDM2 co-crystal structure revealed that both peptides present into the same groove on MDM2 with the same axial direction (N->C), and make use of similar side chains (Figure 5E). Chemically related side chains project with similar orientations for both peptides, perhaps due to the peptides' matched left-handed helices. Matching helicity is not an exclusive requirement to make use of similar side chain interactions, as D-H101 also uses a similar binding mode to the L-peptide MDM2-binder ATSP-7041[51]. The binding mode of ATSP-7041 overlaid onto D-H101 reveals important side-chain interactions (Figure 5F). Despite having oppositely handed helicities, both peptides bind into the same groove on MDM2 in the same direction, and make use of similar side chain interactions.

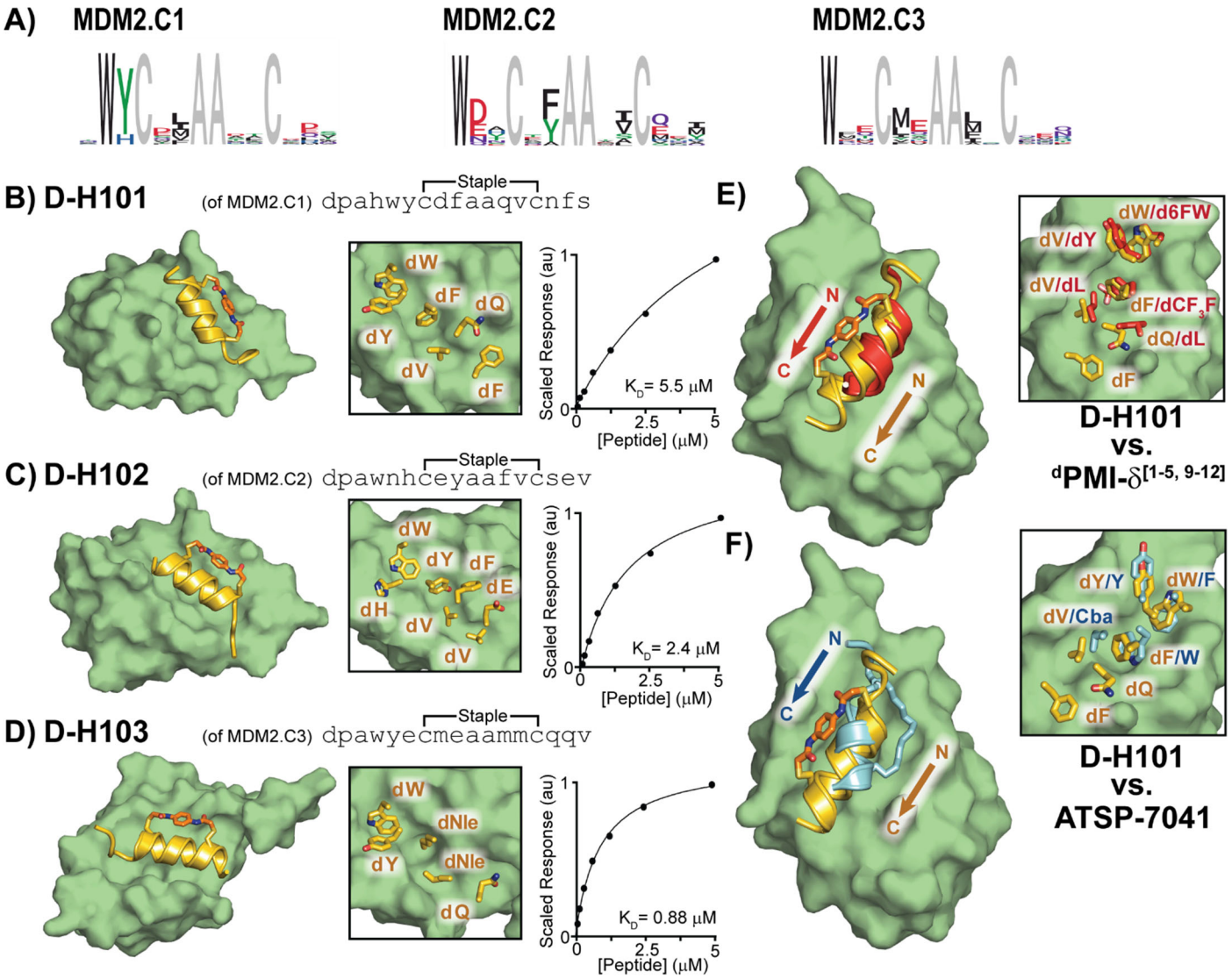

Figure 5. Mirror-image phage display of D-MDM2 generates both novel and previously reported binding motifs. A) Logo plots of the three clusters that bind to MDM2, with fixed residues in grey. **B-D)** For each target, the D-peptide was co-crystallized with recombinant L-MDM2, and the resulting X-ray crystal structure is shown with important side-chain interactions highlighted in the insets. Steady-state SPR sensorgrams are shown with binding affinity values. **E-F)** The co-crystal structure of D-H101 with MDM2 is shown overlaid with known D-peptide binders ^{d}PMI-δ[15,50] (PDB ID: 4NT5) (E) and ATSP-7041[51] (PDB ID: 4N5T) (F). The insets show essential side-chain interactions.

Given the ease with which we identified D-MDM2-binding Helicons, we next applied the phage screening platform to identify Helicons that bind to synthetic D-CHIP that we generated in this work. CHIP is a member of the RING/U-Box family of E3 ligases that catalyze the conjugation of ubiquitin to substrates destined for proteasomal degradation[52]. CHIP recognizes unstructured substrates (typically an (I/M)EEVD motif) through a hydrophobic cleft in its TPR domain[53], but there are no known α-helical, nor mirror-image binders. From the single-round phage screen, we identified three clusters that displayed robust binding to CHIP (CHIP.C1 – CHIP.C3) (Fig 5A, and SI Section 9.2). All three clusters feature conserved terminal residues with carboxylate functionalities (dD3 in CHIP.C1, dD1/dE2 in

CHIP.C2, and dD12 in CHIP.C3), consistent with the conserved terminal D-residues common to known CHIP substrates. As well, hydrophobic residues are retained in the *i*,*i*+4/5 positions relative to the anchoring aspartic acid residue: dW6 in CHIP.C1, dW6 in CHIP.C2, and dA8 in CHIP.C3. To further investigate these binding interactions, we synthesized representative D-peptides from each cluster (D-H201 from CHIP.C1, D-H203 from CHIP.C3, and D-H202 from CHIP.C2) and used a competition fluorescence polarization assay to quantitate the affinity of each D-peptide to recombinant CHIP. In this assay, a peptide with the N-terminal sequence of HSP70 (SSGPTIEEVD) is labeled with FAM at its N-terminus and incubated with recombinant CHIP. Each peptide is added in turn at varying concentrations, and ejection of the FAM labeled peptide is measured as a decrease in fluorescence polarization. Using this assay, the three peptides D-H201, D-D-H203, and D-D-H202 displayed IC_{50} values of 0.47 μM, 0.55 μM, and 1.23 μM, respectively (Fig. 6B-D) (see SI Section 8.12).

To further investigate the nature of the binding modes, we solved the X-ray co-crystal structures of each peptide with recombinant CHIP (Fig. 6B-D, 1.72 Å, 1.59 Å, and 1.76 Å respectively) (see SI Sections 10.2 and 10.4). As predicted, all three peptides form left-handed α-helices to engage the same groove in CHIP, though D-H202 bound in the reverse direction compared to D-201 and D-203 (Fig. 6B-D). The terminal dD/dE residues for each peptide display a similar orientation to each other and to CHIP-Opt, a known unstructured CHIP-binder [53] (Fig. 6B-E). D-H203 and CHIP-Opt also both retain terminal carboxylate-containing residues (dE3/D5), and the hydrophobic contacts of D-203 residues dM4 and dW7 are similar to those of P4 and L1 of CHIP-Opt respectively.

Overall, we demonstrate the successful application of AFPS to generate quantities of D-protein sufficient for high-throughput screening, and ultimate development of D-form α-helical peptides that bind to the therapeutically relevant MDM2 and CHIP proteins.

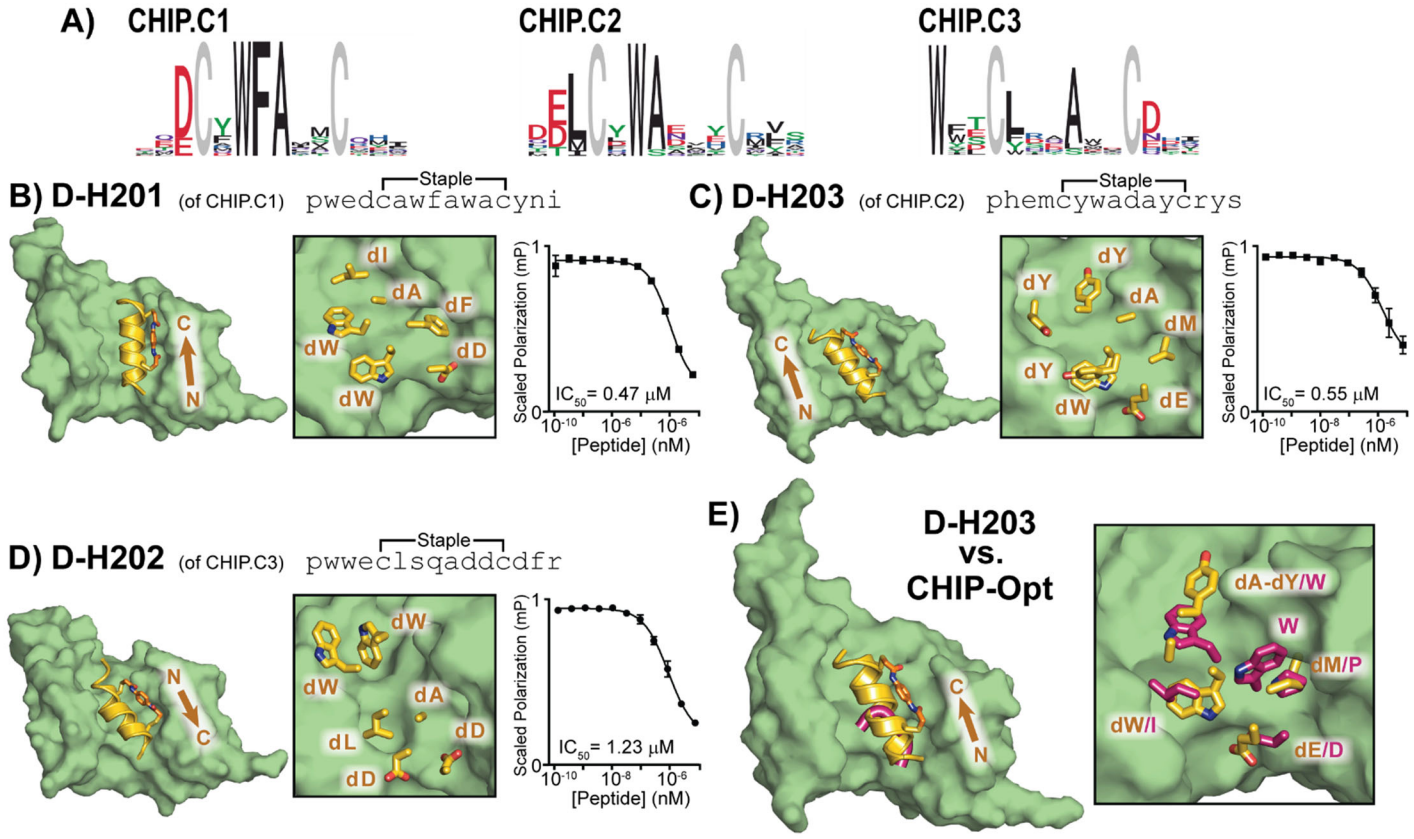

Figure 6. Novel D-peptides identified from MIPD bind to recombinant CHIP. A) Logo plots of each identified binding cluster to D-CHIP are shown. **B-D)** X-ray co-crystal structures of each peptide with recombinant CHIP with insets highlighting important side-chain interactions (left and middle) are shown with competition FP traces for each peptide to FAM-HSP70-peptide bound recombinant CHIP with extracted kinetic constants (right). **E)** The crystal structure of CHIP-Opt (PDB: 6NSV) overlaid onto the D-H203 CHIP co-structure, with an inset highlighting important side chain interactions.

Discussion

One of the largest obstacles to fully realizing the potential of peptide science is the consistent and predictable production of novel protein targets, but sequence-specific complications are ubiquitous. Ultimately, any protein synthesis pipeline should be judged on its ability to manufacture folded proteins of a quality and quantity that is sufficient for the intended application. We leveraged flow synthesis to manufacture 24 folded synthetic proteins – 12 targets produced as both the L- and D-enantiomers. In so doing, we demonstrate that AFPS can form the foundation of a protein production pipeline that does not necessarily require the individual troubleshooting of each synthetic target. For the eight novel protein sequences that we report here, each was produced in a single pass using a standardized synthesis, purification, and folding strategy.

Beyond this achievement, we also set out to determine if the D proteins from the AFPS platform could be integrated into a drug discovery pipeline. Approaches to phage display have advanced greatly in recent years, but newer optimized methods have rarely been applied to the screening of mirror-image proteins. We therefore selected two of the enantiomeric protein pairs generated here (MDM2 and CHIP) and applied these in a newly reported phage display screening platform to identify six families of macrocyclic mirror-image binding motifs, and representative peptides (Helicons) with sub-micromolar binding affinities. As a primary read-out of the validity of our D-proteins from AFPS, we first investigated whether we could rediscover the mirror-image ligands that had already been discovered against the MDM2. Indeed, we discovered three mirror-image clusters, and analysis of x-ray co-crystal structures of each revealed two binding clusters that closely recapitulated binding interactions of both L and D known high affinity binders to MDM2. In addition, the third cluster displayed a previously undiscovered mirror-image binding mode, and efforts are underway to further refine this interaction.

Having validated our screening approach, we turned to a novel target, CHIP, and discovered its first D-peptide binder. We identified three novel mirror-image macrocyclic binding modes and further characterized each with x-ray co-crystal structures of representative D peptides complexed with the recombinant protein. Until now, there were no α-helical binders of CHIP, but interestingly, two of our identified binding motifs, although α-helical, make use of similar binding interactions to known unstructured biological binders. Work is underway to translate these binding motifs into minimized cell-penetrant units for therapeutic applications.

Indeed, hypermodified peptides are an emerging therapeutic scaffold that can address some of the long-standing issues of traditional peptide-based drugs, including their short biological half-lives and poor cell permeability. Macrocyclized D peptides have the potential to address both of these issues[8]. Because they are not recognized by native L-proteases, D peptides display uncommonly long in vivo half lives[54], and as a result are a privileged peptide drug scaffold. In addition, masking of amide hydrogens through macrocyclization as exemplified by the peptide natural products cyclosporin A[55], kalata-b1[56], and the candidate PCSK9 inhibitor MK-0616[57], can impart potent cell permeability. These favorable properties are leading to a renewed interest in these scaffolds for drug discovery efforts, and the rapid generation of macrocyclized D peptide ligands to novel protein targets by AFPS reported here offers a unique approach to advance this emerging field of study.

The rapid generation of high-affinity mirror-image binding modes made possible with AFPS coupled to modern Helicon phage display screening represents a major advance in the practicality of MIPD, and stands to revitalize campaigns to generate mirror-image binders to new and emerging protein targets.

Notes

The authors declare the following competing financial interest(s): B.L.P. is a co-founder and/or member of the scientific advisory board of several companies focusing on the development of protein and peptide therapeutics. T.L.T, K.L., O.S.T., J.M.S., G.L.V., and J.H.M are currently employed by FOG Pharmaceuticals, and G.L.V. serves on the board of directors of FOG Pharmaceuticals. FOG Pharmaceuticals has filed provisional patent applications related to the compounds described in this work.

Acknowledgements

Financial support for this work was provided by FOG Pharmaceuticals (to B.L.P.). We thank Mirella Bucci for her valuable comments during manuscript preparation.

References

(1) Milton, R. C.; Milton, S. C.; Kent, S. B. Total Chemical Synthesis of a D-Enzyme: The Enantiomers of HIV-1 Protease Show Reciprocal Chiral Substrate Specificity [Corrected]. *Science* **1992**, *256* (5062), 1445–1448. https://doi.org/10.1126/science.1604320.

(2) Wang, Z.; Xu, W.; Liu, L.; Zhu, T. F. A Synthetic Molecular System Capable of Mirror-Image Genetic Replication and Transcription. *Nature Chemistry* **2016**, *8* (7), 698–704. https://doi.org/10.1038/nchem.2517.

(3) Xu, Y.; Zhu, T. F. Mirror-Image T7 Transcription of Chirally Inverted Ribosomal and Functional RNAs. *Science* **2022**, *378* (6618), 405–412. https://doi.org/10.1126/science.abm0646.

(4) Fan, C.; Deng, Q.; Zhu, T. F. Bioorthogonal Information Storage in L-DNA with a High-Fidelity Mirror-Image Pfu DNA Polymerase. *Nature Biotechnology* **2021**, *39* (12), 1548–1555. https://doi.org/10.1038/s41587-021-00969-6.

(5) Kent, S. B. H. Novel Protein Science Enabled by Total Chemical Synthesis. *Protein Science* **2019**, *28* (2), 313–328. https://doi.org/10.1002/pro.3533.

(6) Hartrampf, N.; Saebi, A.; Poskus, M.; Gates, Z. P.; Callahan, A. J.; Cowfer, A. E.; Hanna, S.; Antilla, S.; Schissel, C. K.; Quartararo, A. J.; Ye, X.; Mijalis, A. J.; Simon, M. D.; Loas, A.; Liu, S.; Jessen, C.; Nielsen, T. E.; Pentelute, B. L. Synthesis of Proteins by Automated Flow Chemistry. *Science* **2020**, *368* (6494), 980. https://doi.org/10.1126/science.abb2491.

(7) Schumacher, T. N. M.; Mayr, L. M.; Minor, D. L.; Milhollen, M. A.; Burgess, M. W.; Kim, P. S. Identification of D-Peptide Ligands Through Mirror-Image Phage Display. *Science* **1996**, *271* (5257), 1854–1857. https://doi.org/10.1126/science.271.5257.1854.

(8) Muttenthaler, M.; King, G. F.; Adams, D. J.; Alewood, P. F. Trends in Peptide Drug Discovery. *Nature Reviews Drug Discovery* **2021**, *20* (4), 309–325. https://doi.org/10.1038/s41573-020-00135-8.

(9) Eckert, D. M.; Malashkevich, V. N.; Hong, L. H.; Carr, P. A.; Kim, P. S. Inhibiting HIV-1 Entry: Discovery of D-Peptide Inhibitors That Target the Gp41 Coiled-Coil Pocket. *Cell* **1999**, *99* (1), 103–115. https://doi.org/10.1016/S0092-8674(00)80066-5.

(10) Liu, M.; Pazgier, M.; Li, C.; Yuan, W.; Li, C.; Lu, W. A Left-Handed Solution to Peptide Inhibition of the P53–MDM2 Interaction. *Angewandte Chemie International Edition* **2010**, *49* (21), 3649–3652. https://doi.org/10.1002/anie.201000329.

(11) Marinec, P. S.; Landgraf, K. E.; Uppalapati, M.; Chen, G.; Xie, D.; Jiang, Q.; Zhao, Y.; Petriello, A.; Deshayes, K.; Kent, S. B. H.; Ault-Riche, D.; Sidhu, S. S. A Non-Immunogenic Bivalent d-Protein Potently Inhibits Retinal Vascularization and Tumor Growth. *ACS Chem. Biol.* **2021**, *16* (3), 548–556. https://doi.org/10.1021/acschembio.1c00017.

(12) Zhou, X.; Zuo, C.; Li, W.; Shi, W.; Zhou, X.; Wang, H.; Chen, S.; Du, J.; Chen, G.; Zhai, W.; Zhao, W.; Wu, Y.; Qi, Y.; Liu, L.; Gao, Y. A Novel D-Peptide Identified by Mirror-Image Phage Display Blocks TIGIT/PVR for Cancer Immunotherapy. *Angewandte Chemie International Edition* **2020**, *59* (35), 15114–15118. https://doi.org/10.1002/anie.202002783.

(13) Chang, H.-N.; Liu, B.-Y.; Qi, Y.-K.; Zhou, Y.; Chen, Y.-P.; Pan, K.-M.; Li, W.-W.; Zhou, X.-M.; Ma, W.-W.; Fu, C.-Y.; Qi, Y.-M.; Liu, L.; Gao, Y.-F. Blocking of the PD-1/PD-L1 Interaction by a D-Peptide Antagonist for Cancer

Immunotherapy. *Angewandte Chemie International Edition* **2015**, *54* (40), 11760–11764. https://doi.org/10.1002/anie.201506225.
(14) Mandal, K.; Uppalapati, M.; Ault-Riché, D.; Kenney, J.; Lowitz, J.; Sidhu, S. S.; Kent, S. B. H. Chemical Synthesis and X-Ray Structure of a Heterochiral {D-Protein Antagonist plus Vascular Endothelial Growth Factor} Protein Complex by Racemic Crystallography. *Proceedings of the National Academy of Sciences* **2012**, *109* (37), 14779–14784. https://doi.org/10.1073/pnas.1210483109.
(15) Liu, M.; Li, C.; Pazgier, M.; Li, C.; Mao, Y.; Lv, Y.; Gu, B.; Wei, G.; Yuan, W.; Zhan, C.; Lu, W.-Y.; Lu, W. D-Peptide Inhibitors of the P53–MDM2 Interaction for Targeted Molecular Therapy of Malignant Neoplasms. *PNAS* **2010**, *107* (32), 14321–14326. https://doi.org/10.1073/pnas.1008930107.
(16) Huang, L.; Xie, J.; Bi, Q.; Li, Z.; Liu, S.; Shen, Q.; Li, C. Highly Selective Targeting of Hepatic Stellate Cells for Liver Fibrosis Treatment Using a D-Enantiomeric Peptide Ligand of Fn14 Identified by Mirror-Image MRNA Display. *Mol. Pharmaceutics* **2017**, *14* (5), 1742–1753. https://doi.org/10.1021/acs.molpharmaceut.6b01174.
(17) Li, Z.; Xie, J.; Peng, S.; Liu, S.; Wang, Y.; Lu, W.; Shen, J.; Li, C. Novel Strategy Utilizing Extracellular Cysteine-Rich Domain of Membrane Receptor for Constructing d-Peptide Mediated Targeted Drug Delivery Systems: A Case Study on Fn14. *Bioconjugate Chem.* **2017**, *28* (8), 2167–2179. https://doi.org/10.1021/acs.bioconjchem.7b00326.
(18) Díaz-Perlas, C.; Varese, M.; Guardiola, S.; Sánchez-Navarro, M.; García, J.; Teixidó, M.; Giralt, E. Protein Chemical Synthesis Combined with Mirror-Image Phage Display Yields d-Peptide EGF Ligands That Block the EGF–EGFR Interaction. *ChemBioChem* **2019**, *20* (16), 2079–2084. https://doi.org/10.1002/cbic.201900355.
(19) Wiesehan, K.; Buder, K.; Linke, R. P.; Patt, S.; Stoldt, M.; Unger, E.; Schmitt, B.; Bucci, E.; Willbold, D. Selection of D-Amino-Acid Peptides That Bind to Alzheimer's Disease Amyloid Peptide Aβ1–42 by Mirror Image Phage Display. *ChemBioChem* **2003**, *4* (8), 748–753. https://doi.org/10.1002/cbic.200300631.
(20) El-Faham, A.; Albericio, F. Peptide Coupling Reagents, More than a Letter Soup. *Chemical Reviews*, 2011, *111*, 6557–6602. https://doi.org/10.1021/cr100048w.
(21) Dawson, P. E.; Kent, S. B. H. Synthesis of Native Proteins by Chemical Ligation. *Annu. Rev. Biochem.* **2000**, *69* (1), 923–960. https://doi.org/10.1146/annurev.biochem.69.1.923.
(22) Mijalis, A. J.; Thomas Iii, D. A.; Simon, M. D.; Adamo, A.; Beaumont, R.; Jensen, K. F.; Pentelute, B. L. A Fully Automated Flow-Based Approach for Accelerated Peptide Synthesis. *Nature Chemical Biology*, 2017, *13*, 464. https://doi.org/10.1038/nchembio.2318 https://www.nature.com/articles/nchembio.2318#supplementary-information.
(23) Zuo, C.; Zhang, B.; Wu, M.; Bierer, D.; Shi, J.; Fang, G.-M. Chemical Synthesis and Racemic Crystallization of Rat C5a-DesArg. *Chinese Chemical Letters* **2020**, *31* (3), 693–696. https://doi.org/10.1016/j.cclet.2019.08.039.
(24) Ling, J.-J.; Fan, C.; Qin, H.; Wang, M.; Chen, J.; Wittung-Stafshede, P.; Zhu, T. F. Mirror-Image 5S Ribonucleoprotein Complexes. *Angewandte Chemie International Edition* **2020**, *59* (9), 3724–3731. https://doi.org/10.1002/anie.201914799.
(25) Zuo, C.; Shi, W.-W.; Chen, X.-X.; Glatz, M.; Riedl, B.; Flamme, I.; Pook, E.; Wang, J.; Fang, G.-M.; Bierer, D.; Liu, L. Chimeric Protein Probes for C5a Receptors through Fusion of the Anaphylatoxin C5a Core Region with a Small-Molecule Antagonist. *Science China Chemistry* **2019**, *62* (10), 1371–1378. https://doi.org/10.1007/s11426-019-9513-2.
(26) Weidmann, J.; Schnölzer, M.; Dawson, P. E.; Hoheisel, J. D. Copying Life: Synthesis of an Enzymatically Active Mirror-Image DNA-Ligase Made of D-Amino Acids. *Cell Chemical Biology* **2019**, *26* (5), 645-651.e3. https://doi.org/10.1016/j.chembiol.2019.02.008.
(27) Shu, K.; Iwamoto, N.; Honda, K.; Kondoh, Y.; Hirano, H.; Osada, H.; Ohno, H.; Fujii, N.; Oishi, S. Development of Mirror-Image Screening Systems for XIAP BIR3 Domain Inhibitors. *Bioconjugate Chem.* **2019**, *30* (5), 1395–1404. https://doi.org/10.1021/acs.bioconjchem.9b00154.
(28) Wang, M.; Jiang, W.; Liu, X.; Wang, J.; Zhang, B.; Fan, C.; Liu, L.; Pena-Alcantara, G.; Ling, J.-J.; Chen, J.; Zhu, T. F. Mirror-Image Gene Transcription and Reverse Transcription. *Chem* **2019**, *5* (4), 848–857. https://doi.org/10.1016/j.chempr.2019.01.001.
(29) Guo, Q.-Y.; Zhang, L.-H.; Zuo, C.; Huang, D.-L.; Wang, Z. A.; Zheng, J.-S.; Tian, C.-L. Channel Activity of Mirror-Image M2 Proton Channel of Influenza A Virus Is Blocked by Achiral or Chiral Inhibitors. *Protein & Cell* **2019**, *10* (3), 211–216. https://doi.org/10.1007/s13238-018-0536-5.
(30) De Rosa, L.; Di Stasi, R.; D'Andrea, L. D. Total Chemical Synthesis by Native Chemical Ligation of the All-D Immunoglobulin-like Domain 2 of Axl. *Tetrahedron* **2019**, *75* (7), 894–905. https://doi.org/10.1016/j.tet.2019.01.005.
(31) Chen, C.-C.; Gao, S.; Ai, H.-S.; Qu, Q.; Tian, C.-L.; Li, Y.-M. Racemic X-Ray Structure of L-Type Calcium Channel Antagonist Calciseptine Prepared by Total Chemical Synthesis. *Science China Chemistry* **2018**, *61* (6), 702–707. https://doi.org/10.1007/s11426-017-9198-y.
(32) Levinson, A. M.; McGee, J. H.; Roberts, A. G.; Creech, G. S.; Wang, T.; Peterson, M. T.; Hendrickson, R. C.; Verdine, G. L.; Danishefsky, S. J. Total Chemical Synthesis and Folding of All-l and All-d Variants of Oncogenic KRas(G12V). *Journal of the American Chemical Society*, 2017, *139*, 7632–7639. https://doi.org/10.1021/jacs.7b02988.
(33) Pech, A.; Achenbach, J.; Jahnz, M.; Schülzchen, S.; Jarosch, F.; Bordusa, F.; Klussmann, S. A Thermostable D-Polymerase for Mirror-Image PCR. *Nucleic Acids Research* **2017**, *45* (7), 3997–4005. https://doi.org/10.1093/nar/gkx079.

(34) Xu, W.; Jiang, W.; Wang, J.; Yu, L.; Chen, J.; Liu, X.; Liu, L.; Zhu, T. F. Total Chemical Synthesis of a Thermostable Enzyme Capable of Polymerase Chain Reaction. *Cell Discovery* **2017**, *3* (1), 17008. https://doi.org/10.1038/celldisc.2017.8.
(35) Noguchi, T.; Ishiba, H.; Honda, K.; Kondoh, Y.; Osada, H.; Ohno, H.; Fujii, N.; Oishi, S. Synthesis of Grb2 SH2 Domain Proteins for Mirror-Image Screening Systems. *Bioconjugate Chem.* **2017**, *28* (2), 609–619. https://doi.org/10.1021/acs.bioconjchem.6b00692.
(36) Shu, K.; Noguchi, T.; Honda, K.; Kondoh, Y.; Osada, H.; Ohno, H.; Fujii, N.; Oishi, S. Synthesis of the Src SH2 Domain and Its Application in Bioassays for Mirror-Image Screening. *RSC Adv.* **2017**, *7* (61), 38725–38732. https://doi.org/10.1039/C7RA07445J.
(37) Guo, C.; Zhang, L.-Q.; Jiang, W. Biodegrading Plastics with a Synthetic Non-Biodegradable Enzyme. *Chem*. https://doi.org/10.1016/j.chempr.2022.09.008.
(38) Li, K.; Tokareva, O. S.; Thomson, T. M.; Wahl, S. C. T.; Travaline, T. L.; Ramirez, J. D.; Choudary, S. K.; Agarwal, S.; Walkup, W. G.; Olsen, T. J.; Brennan, M. J.; Verdine, G. L.; McGee, J. H. De Novo Mapping of α-Helix Recognition Sites on Protein Surfaces Using Unbiased Libraries. *Proceedings of the National Academy of Sciences* **2022**, *119* (52), e2210435119. https://doi.org/10.1073/pnas.2210435119.
(39) Vinogradov, A. A.; Evans, E. D.; Pentelute, B. L. Total Synthesis and Biochemical Characterization of Mirror Image Barnase. *Chem. Sci.* **2015**, *6* (5), 2997–3002. https://doi.org/10.1039/C4SC03877K.
(40) Jbara, M.; Pomplun, S.; Schissel, C. K.; Hawken, S. W.; Boija, A.; Klein, I.; Rodriguez, J.; Buchwald, S. L.; Pentelute, B. L. Engineering Bioactive Dimeric Transcription Factor Analogs via Palladium Rebound Reagents. *J. Am. Chem. Soc.* **2021**, *143* (30), 11788–11798. https://doi.org/10.1021/jacs.1c05666.
(41) Guo, B.; Audu, C. O.; Cochran, J. C.; Mierke, D. F.; Pellegrini, M. Protein Engineering of the N-Terminus of NEMO: Structure Stabilization and Rescue of IKKβ Binding. *Biochemistry* **2014**, *53* (43), 6776–6785. https://doi.org/10.1021/bi500861x.
(42) Jumper, J.; Evans, R.; Pritzel, A.; Green, T.; Figurnov, M.; Ronneberger, O.; Tunyasuvunakool, K.; Bates, R.; Žídek, A.; Potapenko, A.; Bridgland, A.; Meyer, C.; Kohl, S. A. A.; Ballard, A. J.; Cowie, A.; Romera-Paredes, B.; Nikolov, S.; Jain, R.; Adler, J.; Back, T.; Petersen, S.; Reiman, D.; Clancy, E.; Zielinski, M.; Steinegger, M.; Pacholska, M.; Berghammer, T.; Bodenstein, S.; Silver, D.; Vinyals, O.; Senior, A. W.; Kavukcuoglu, K.; Kohli, P.; Hassabis, D. Highly Accurate Protein Structure Prediction with AlphaFold. *Nature* **2021**, *596* (7873), 583–589. https://doi.org/10.1038/s41586-021-03819-2.
(43) Varadi, M.; Anyango, S.; Deshpande, M.; Nair, S.; Natassia, C.; Yordanova, G.; Yuan, D.; Stroe, O.; Wood, G.; Laydon, A.; Žídek, A.; Green, T.; Tunyasuvunakool, K.; Petersen, S.; Jumper, J.; Clancy, E.; Green, R.; Vora, A.; Lutfi, M.; Figurnov, M.; Cowie, A.; Hobbs, N.; Kohli, P.; Kleywegt, G.; Birney, E.; Hassabis, D.; Velankar, S. AlphaFold Protein Structure Database: Massively Expanding the Structural Coverage of Protein-Sequence Space with High-Accuracy Models. *Nucleic Acids Research* **2022**, *50* (D1), D439–D444. https://doi.org/10.1093/nar/gkab1061.
(44) Zhan, C.; Varney, K.; Yuan, W.; Zhao, L.; Lu, W. Interrogation of MDM2 Phosphorylation in P53 Activation Using Native Chemical Ligation: The Functional Role of Ser17 Phosphorylation in MDM2 Reexamined. *J. Am. Chem. Soc.* **2012**, *134* (15), 6855–6864. https://doi.org/10.1021/ja301255n.
(45) Rushe, M.; Silvian, L.; Bixler, S.; Chen, L. L.; Cheung, A.; Bowes, S.; Cuervo, H.; Berkowitz, S.; Zheng, T.; Guckian, K.; Pellegrini, M.; Lugovskoy, A. Structure of a NEMO/IKK-Associating Domain Reveals Architecture of the Interaction Site. *Structure* **2008**, *16* (5), 798–808. https://doi.org/10.1016/j.str.2008.02.012.
(46) Yang, Y.; Xu, Z.; He, C.; Zhang, B.; Shi, Y.; Li, F. Structural Insights into the Recognition of γ-Globin Gene Promoter by BCL11A. *Cell Research* **2019**, *29* (11), 960–963. https://doi.org/10.1038/s41422-019-0221-0.
(47) Kelemen, B. R.; Klink, T. A.; Behike, M. A.; Eubanks, S. R.; Leland, P. A.; Raines, R. T. Hypersensitive Substrate for Ribonucleases. *Nucleic Acids Research* **1999**, *27* (18), 3696–3701. https://doi.org/10.1093/nar/27.18.3696.
(48) Mackereth, C. D.; Schärpf, M.; Gentile, L. N.; MacIntosh, S. E.; Slupsky, C. M.; McIntosh, L. P. Diversity in Structure and Function of the Ets Family PNT Domains. *Journal of Molecular Biology* **2004**, *342* (4), 1249–1264. https://doi.org/10.1016/j.jmb.2004.07.094.
(49) Lin, S.-C.; Lo, Y.-C.; Wu, H. Helical Assembly in the MyD88–IRAK4–IRAK2 Complex in TLR/IL-1R Signalling. *Nature* **2010**, *465* (7300), 885–890. https://doi.org/10.1038/nature09121.
(50) Kannan, S.; Aronica, P. G. A.; Ng, S.; Gek Lian, D. T.; Frosi, Y.; Chee, S.; Shimin, J.; Yuen, T. Y.; Sadruddin, A.; Kaan, H. Y. K.; Chandramohan, A.; Wong, J. H.; Tan, Y. S.; Chang, Z. W.; Ferrer-Gago, F. J.; Arumugam, P.; Han, Y.; Chen, S.; Rénia, L.; Brown, C. J.; Johannes, C. W.; Henry, B.; Lane, D. P.; Sawyer, T. K.; Verma, C. S.; Partridge, A. W. Macrocyclization of an All-d Linear α-Helical Peptide Imparts Cellular Permeability. *Chem. Sci.* **2020**, *11* (21), 5577–5591. https://doi.org/10.1039/C9SC06383H.
(51) Chang, Y. S.; Graves, B.; Guerlavais, V.; Tovar, C.; Packman, K.; To, K.-H.; Olson, K. A.; Kesavan, K.; Gangurde, P.; Mukherjee, A.; Baker, T.; Darlak, K.; Elkin, C.; Filipovic, Z.; Qureshi, F. Z.; Cai, H.; Berry, P.; Feyfant, E.; Shi, X. E.; Horstick, J.; Annis, D. A.; Manning, A. M.; Fotouhi, N.; Nash, H.; Vassilev, L. T.; Sawyer, T. K. Stapled A−helical Peptide Drug Development: A Potent Dual Inhibitor of MDM2 and MDMX for P53-Dependent Cancer Therapy. *Proc Natl Acad Sci USA* **2013**, *110* (36), E3445–E3454. https://doi.org/10.1073/pnas.1303002110.
(52) Jiang, J.; Ballinger, C. A.; Wu, Y.; Dai, Q.; Cyr, D. M.; Höhfeld, J.; Patterson, C. CHIP Is a U-Box-Dependent E3 Ubiquitin Ligase: IDENTIFICATION OF Hsc70 AS A TARGET FOR UBIQUITYLATION *. *Journal of Biological Chemistry* **2001**, *276* (46), 42938–42944. https://doi.org/10.1074/jbc.M101968200.

(53) Ravalin, M.; Theofilas, P.; Basu, K.; Opoku-Nsiah, K. A.; Assimon, V. A.; Medina-Cleghorn, D.; Chen, Y.-F.; Bohn, M. F.; Arkin, M.; Grinberg, L. T.; Craik, C. S.; Gestwicki, J. E. Specificity for Latent C Termini Links the E3 Ubiquitin Ligase CHIP to Caspases. *Nature Chemical Biology* **2019**, *15* (8), 786–794. https://doi.org/10.1038/s41589-019-0322-6.

(54) Kremsmayr, T.; Aljnabi, A.; Blanco-Canosa, J. B.; Tran, H. N. T.; Emidio, N. B.; Muttenthaler, M. On the Utility of Chemical Strategies to Improve Peptide Gut Stability. *J. Med. Chem.* **2022**, acs.jmedchem.2c00094. https://doi.org/10.1021/acs.jmedchem.2c00094.

(55) Bockus, A. T.; Lokey, R. S. Bioactive and Membrane-Permeable Cyclic Peptide Natural Products. In *Practical Medicinal Chemistry with Macrocycles*; 2017; pp 101–132. https://doi.org/10.1002/9781119092599.ch5.

(56) Henriques, S. T.; Huang, Y.-H.; Chaousis, S.; Sani, M.-A.; Poth, A. G.; Separovic, F.; Craik, D. J. The Prototypic Cyclotide Kalata B1 Has a Unique Mechanism of Entering Cells. *Chemistry & Biology* **2015**, *22* (8), 1087–1097. https://doi.org/10.1016/j.chembiol.2015.07.012.

(57) Tucker, T. J.; Embrey, M. W.; Alleyne, C.; Amin, R. P.; Bass, A.; Bhatt, B.; Bianchi, E.; Branca, D.; Bueters, T.; Buist, N.; Ha, S. N.; Hafey, M.; He, H.; Higgins, J.; Johns, D. G.; Kerekes, A. D.; Koeplinger, K. A.; Kuethe, J. T.; Li, N.; Murphy, B.; Orth, P.; Salowe, S.; Shahripour, A.; Tracy, R.; Wang, W.; Wu, C.; Xiong, Y.; Zokian, H. J.; Wood, H. B.; Walji, A. A Series of Novel, Highly Potent, and Orally Bioavailable Next-Generation Tricyclic Peptide PCSK9 Inhibitors. *J. Med. Chem.* **2021**, *64* (22), 16770–16800. https://doi.org/10.1021/acs.jmedchem.1c01599.